Received: 20 March 2018 | Revised: 4 October 2018 | Accepted: 27 October 2018

DOI: 10.1002/stc.2293

RESEARCH ARTICLE

WILEY

Baseline-free multidamage identification in plate-like structures by using multiscale approach and low-rank modelling

Shancheng Cao[1] | Huajiang Ouyang[2] | Li Cheng[1]

[1] Department of Mechanical Engineering, Hong Kong Polytechnic University, Kowloon, Hong Kong

[2] Centre for Engineering Dynamics, School of Engineering, University of Liverpool, Liverpool, UK

Correspondence
Huajiang Ouyang, Centre for Engineering Dynamics, School of Engineering, University of Liverpool, Liverpool, L69 3GH, UK.
Email: h.ouyang@liverpool.ac.uk

Summary

Damage localisation based on structural characteristic deflection shapes (CDSs) or their spatial derivatives has been widely investigated due to their high sensitivity to local damage. Despite substantial advances in this kind of methods, several key problems must be addressed to boost their practical applications. This paper deals with three vital issues: their susceptibility to measurement noise, absence of baseline data on pristine structures, and their low effectiveness in identification of multiple damage. To tackle these problems, a statistical baseline-free multidamage identification method is proposed for plate-type structures. In this method, a Laplacian of Gaussian (LoG) filter is adopted to enhance the noise-robustness of the estimated curvatures of CDSs. Without the baseline data on pristine structures, a robust principal component analysis (PCA) is proposed to extract the damage-induced local features by using only the CDS curvatures of the damaged structure. Moreover, a robust multidamage index is defined, which has the capability of integrating the damage information of several CDSs. Finally, the feasibility and the effectiveness of LoG filter, robust PCA, and the proposed multidamage index are validated by using both numerical and experimental studies of plates with two damage zones. It is found that the two damage zones with only 10% thickness reduction can be accurately detected and localised by using the proposed multidamage identification method.

KEYWORDS

Laplacian of Gaussian, mode shape curvatures, multidamage identification, robust principal component analysis

1 | INTRODUCTION

With the wide-spread use of metallic and composite structures in modern society, a major challenge is to secure their normal operation by inspection and maintenance.[1-3] Among various non-destructive structural health monitoring techniques, vibration-based methods have been widely applied in aerospace, civil, and mechanical systems, as they are capable of

providing both global and local damage features.[4,5] Generally, vibration-based methods can be categorised according to different criteria such as levels of damage identification, linear or nonlinear vibration responses, and whether using physics-based models or not.[6-8]

Generally speaking, there are fewer papers on damage identification of plates than of beams. Recently, damage identification in plates has attracted more attention.[9-14] Instead of natural frequencies, structural characteristic deflection shapes (CDSs) or their spatial derivatives are commonly used to reveal the local damage features.[15-17] Here, CDSs refer to shape features that possess structural spatial deflection information such as mode shapes and operational deflection shapes. The fundamental idea behind this kind of methods is that CDSs or their spatial derivatives contain the damage-induced local shape singularities, which makes them more sensitive to damage than the traditional natural frequency-based methods.[18-20] Moreover, CDSs tend to be much more robust to environmental variability such as temperature or humidity, when compared with natural frequencies. Nevertheless, one disadvantage is that the acquisition of CDSs requires a relatively large number of measurement points. Experiments based on traditional accelerometers are time-consuming, and it is hard to obtain sufficient spatial resolution for CDSs. With the advanced measurement devices such as scanning laser vibrometer (SLV) and full-field digital image correlation, mode shapes or operational deflection shapes are readily acquired at a high-spatial resolution within a short time.[21-24]

For CDS-based damage identification, the high-order derivatives of CDSs such as the curvature are more sensitive to damage, as they effectively amplify the damage-induced local structural changes. However, the estimation of CDS derivatives by using the finite difference method is vulnerable to measurement noise.[25,26] To alleviate the effects of measurement noise on CDSs or their spatial derivatives, statistical approaches, smoothing techniques, or wavelet transform are typically used.[27-29]

The CDS- or its spatial derivative-based damage identification can be either baseline-based or baseline-free. When the baseline data of the healthy state is available, Pandey et al.[30] demonstrated that the absolute changes in mode shape curvature before and after damage were an efficient damage indicator. Hu and Afzal[31] proposed a statistical algorithm for damage detection in timber beam structures using the differences of the curvature mode shapes before and after damage. Wahab and De Roeck[32] combined the curvature differences before and after damage of several modes for damage identification and this method was validated by localising damage in a real bridge.

In practice, baseline data on pristine structures may not be available. In this case, advanced signal processing techniques are harnessed to examine the damage-induced local singularities of CDSs or their spatial derivatives of damaged structures. These advanced signal processing approaches can be classified into two categories. One category uses methods such as wavelet analysis, fractal dimension analysis, and Teager energy operator to reveal the sudden changes or peaks of CDSs or CDS spatial derivatives for damage localisation.[33] Cao et al.[34] investigated the application of complex-wavelet analysis of mode shape curvatures of beam-type structures for multicrack detection, and this method was verified to be noise robust and accurate. Xu et al.[27] improved the curvature mode shape estimation of plates by estimating an equivalent mode shape curvature using Mexican hat wavelet. Then, the Teager energy operator was applied to indicate the local singularities for damage localisation.

The other category aims to construct the pseudo-CDSs or CDS spatial derivatives of the healthy state based on those of the damaged state via surrogate models or low-rank models. The basic idea is that the CDSs or their spatial derivatives of an intact plate are smooth or, when arranged into a matrix by following the measurement grid, possess a low-rank structure (which means that this is a low-rank matrix). Then, the differences between the original CDSs (or CDS spatial derivatives) and constructed CDSs (or CDS spatial derivatives) are used to indicate the damage. The advantage of this kind of methods is that the damage information of several CDSs can be combined effectively for a robust multidamage identification. Yoon et al.[35] extended the gapped smoothing method to the two-dimensional plates, and damage localisation was achieved by examining the singularities in mode shape curvatures. Xu and Zhu[9] applied a global polynomial fitting method to construct the mode shapes of the healthy state based on the mode shapes of the damaged state. Then the square of the differences between them was used to locate the damage. Yang et al.[36] investigated the low-rank modelling for damage identification in plates based on the simulated strain field. The damage detection results showed that it was feasible to localise the damage by using low-resolution strain measurements.

For practical engineering structures, the baseline data on pristine structures is rarely available or hard to obtain. Moreover, the acquired CDSs in experiments are easily contaminated by measurement noise, and the evaluation of high-order CDS spatial derivatives further amplifies the noise effects. In addition, multidamage identification cannot be accomplished by using a single CDS, as a single CDS is just sensitive to damage at some regions while insensitive to damage at other regions.[37] To address these problems, a statistical baseline-free multidamage localisation method is proposed for robust damage identification in plates. Different with the baseline-free methods that directly use the sudden changes

or peaks in CDSs or CDS spatial derivatives for damage localisation, the proposed method extracts the damage-induced local singularities in CDS curvatures of the damaged state. Furthermore, the extracted damage information of each CDS is normalised based on a statistical criterion before being integrated in the proposed multidamage index.

The structure of this paper is outlined as follows. In Section 2, a multiscale approach, Laplacian of Gaussian (LoG) filter, is investigated to guarantee the noise robustness and accuracy of the estimated mode shape curvatures. Then, a robust principal component analysis (PCA) is employed to extract the damage-induced singularities of mode shape curvatures without requiring baseline data of the healthy state in Section 3. In Section 4, a robust multidamage localisation index is proposed for plate-type structures, which fairly incorporates the damage information of several modes. Numerical and experimental studies are conducted to validate the proposed baseline-free multidamage identification method in Section 5 and Section 6, respectively. Finally, some key conclusions are summarised in Section 7.

2 | ROBUST CURVATURE ESTIMATION VIA LoG FILTER

For a homogeneous thin plate with a constant thickness, the relationship between the moments and plate deflection is expressed in Equation (1) according to the Kirchhoff plate theory:

$$\begin{bmatrix} M_x \\ M_y \\ M_{xy} \end{bmatrix} = -\frac{Eh^3}{12(1-\upsilon^2)} \begin{bmatrix} 1 & \upsilon & 0 \\ \upsilon & 1 & 0 \\ 0 & 0 & 1-\upsilon \end{bmatrix} \begin{bmatrix} \dfrac{\partial^2 w}{\partial x^2} \\ \dfrac{\partial^2 w}{\partial y^2} \\ \dfrac{\partial^2 w}{\partial x \partial y} \end{bmatrix}, \tag{1}$$

where M_x and M_y are the bending moments in the x and y directions, respectively, and M_{xy} is the torsional moment. $D = \dfrac{Eh^3}{12(1-\upsilon^2)}$ is the plate's flexural rigidity with Young's modulus E, the thickness of the plate h, and the Poisson's ratio υ. $w(x,y)$ is the plate displacement in the z direction.

In the case of damage, the plate flexural rigidity D of damaged region normally decreases due to the reduction of Young's modulus E or the plate thickness h that caused by the presence of damage. For damage identification in plates, the curvatures of plate deflections are commonly utilised due to their higher sensitivity when compared with CDSs. Normally, the mode shape curvatures are approximated by the second-order partial derivatives due to the small slope assumption, which are estimated via the second-order central difference as

$$\begin{aligned} \Phi_{xx}\left(x_i, y_j\right) &= \frac{\Phi\left(x_{i+1}, y_j\right) - 2\Phi\left(x_i, y_j\right) + \Phi\left(x_{i-1}, y_j\right)}{d_x^2}, \\ \Phi_{yy}\left(x_i, y_j\right) &= \frac{\Phi\left(x_i, y_{j+1}\right) - 2\Phi\left(x_i, y_j\right) + \Phi\left(x_i, y_{j-1}\right)}{d_y^2}, \end{aligned} \tag{2}$$

where Φ_{xx} and Φ_{yy} denote the second-order partial mode shape curvatures along x and y directions, respectively. d_x and d_y represent the grid distances along the x and y directions.

It is worth noting that the second-order central difference method severely amplifies the effects of measurement noise, which degrades the effectiveness and accuracy of damage identification.[38] Hence, the reduction of measurement noise during curvature estimation should be addressed before damage identification.

Multiscale approaches such as Gaussian smoothing and wavelet transform are able to process the original mode shape data at different scales. At a certain scale σ, the measurement noise and local shape details of the original mode shape will be suppressed, and the mode shape so processed becomes smooth. To smoothen the noisy mode shape $\Phi(x,y)$, Gaussian smoothing is applied, which convolves the mode shape $\Phi(x,y)$ with a Gaussian function at a certain scale σ. Moreover, the selection of the scale parameter value is calibrated with numerical simulations in Section 5.

$$L(x,y;\sigma) = \Phi(x,y) \bigotimes g(x,y;\sigma) = \int_{-\infty}^{+\infty}\int_{-\infty}^{+\infty} \Phi(x-u, y-v) g(u,v;\sigma) \mathrm{d}u\mathrm{d}v, \tag{3}$$

where σ denotes the standard deviation of Gaussian function, $\bigotimes$ represents convolution operator, and $g(x,y;\sigma)$ is a Gaussian function. For the two-dimensional applications, an isotropic Gaussian smoothing function is rotationally symmetric and has the form of $g(x,y;\sigma)=\frac{1}{2\pi\sigma^2}e^{-\left(\frac{x^2+y^2}{2\sigma^2}\right)}$.

Inspired by the blob detection in computer vision, the LoG is employed to enhance the mode shape curvature estimation and the associated damage identification accuracy of plate-type structures.[39] A blob represents a region of an image inside which some properties are constant or approximately constant. The Laplacian operator of $L(x,y;\sigma)$ is used to implement the curvature estimation of mode shapes as

$$\nabla^2 L(x,y;\sigma)=\nabla^2(\Phi(x,y)\bigotimes g(x,y;\sigma)), \tag{4}$$

where $\nabla^2=\frac{\partial^2}{\partial x^2}+\frac{\partial^2}{\partial y^2}$ represents the Laplacian operator.

Due to differentiation property of the convolution integral, the Laplacian of $L(x,y;\sigma)$ is equivalent to convolving the original mode shape function $\Phi(x,y)$ with a LoG filter $\nabla^2 g(x,y;\sigma)$, which is expressed as

$$\nabla^2 L(x,y;\sigma)=\nabla^2\Phi(x,y)\bigotimes g(x,y;\sigma)=\Phi(x,y)\bigotimes\nabla^2 g(x,y;\sigma). \tag{5}$$

Equation (5) indicates that the direct application of the second-order central difference approach to $\Phi(x,y)$ can be avoided by using a LoG filter. Furthermore, the effects of measurement noise on the mode shape curvature can be tuned by adjusting the scale parameter σ. In addition, the LoG filter in Equation (5) is written as

$$\nabla^2 g(x,y;\sigma)=-\frac{1}{\pi\sigma^4}\left(1-\frac{x^2+y^2}{2\sigma^2}\right)e^{-\left(\frac{x^2+y^2}{2\sigma^2}\right)}. \tag{6}$$

In this paper, the mean curvature $\Phi_p''=\left(\Phi_{xx}+\Phi_{yy}\right)/2$ is used for damage identification because the sum of the curvatures along two Cartesian coordinate systems sharing the same origin is invariant, which is shown as

$$\begin{cases}\Phi_{x'x'}=\Phi_{xx}\cos^2(\theta)+\Phi_{yy}\sin^2(\theta)+\Phi_{xy}\sin(2\theta)\\ \Phi_{y'y'}=\Phi_{xx}\sin^2(\theta)+\Phi_{yy}\cos^2(\theta)-\Phi_{xy}\sin(2\theta)\end{cases}, \tag{7}$$

where $x'-y'$ indicates a new coordinate system, and it has an angle θ from $x-y$ coordinate system.

3 | LOW-RANK MODELS FOR DAMAGE IDENTIFICATION

Low-rank modelling refers to a group of methods that solve problems by using low-rank property of the original data. For instance, PCA is a well-known low-rank approach, which approximates the original dataset by using the first several principal components. Moreover, matrix completion and robust PCA are powerful approaches for low-rank matrix recovery. Matrix completion is typically used to recover a matrix based on a small number of observed entries, which could be applied to recover the missing data in experiments. Robust PCA can recover a low-dimensional subspace from grossly corrupted data whereas the traditional PCA is vulnerably affected by the gross errors in the original dataset.[40,41]

3.1 | Principal component analysis

For plate-type structures, the mode shape and its curvature of a two-dimensional grid are represented by matrices $\mathbf{\Phi}_p$ and $\mathbf{\Phi}_p''$, respectively. The problem of decomposing $\mathbf{\Phi}_p''^{d}$ into a low-rank matrix $\mathbf{L}$ and a small perturbation matrix $\mathbf{E}$ is

$$\begin{gathered}\mathbf{\Phi}_p''^{d}=\mathbf{L}+\mathbf{E}\\ \text{minimise}\left\|\mathbf{\Phi}_p''^{d}-\mathbf{L}\right\|\ \text{ subject to }\ \text{rank}(\mathbf{L})\le k,\end{gathered} \tag{8}$$

where $\mathbf{\Phi}_{\mathrm{p}}^{''\mathrm{d}}$ is the mode shape curvature of the damaged state, denoted by a superscript d. $\mathbf{L}$ can be considered as an estimation of mode shape curvature $\mathbf{\Phi}_{\mathrm{p}}^{''}$ of the heathy state whereas $\mathbf{E}$ consists of damage information and measurement noise.

Equation (8) can be efficiently solved via singular value decomposition and the singular value decomposition of $\mathbf{\Phi}_{\mathrm{p}}^{''\mathrm{d}} \in \mathbb{R}^{n_1 \times n_2}$ (provided that $n_1 \geq n_2$) is written as

$$\mathbf{\Phi}_{\mathrm{p}}^{''\mathrm{d}} = \mathbf{U}\mathbf{\Sigma}\mathbf{V}^{\mathrm{T}}, \tag{9}$$

in which $\mathbf{U}=[\mathbf{u}_1, \mathbf{u}_2, \cdots, \mathbf{u}_{n_1}] \in \mathbb{R}^{n_1 \times n_1}$ and $\mathbf{V}=[\mathbf{v}_1, \mathbf{v}_2, \cdots, \mathbf{v}_{n_2}] \in \mathbb{R}^{n_2 \times n_2}$ are the orthogonal matrices, and $\mathbf{\Sigma} \in \mathbb{R}^{n_1 \times n_2}$ is a non-negative rectangular diagonal matrix with top n_2 rows containing singular values in a descending order: $\lambda_1 \geq \lambda_2 \geq \cdots \geq \lambda_{n_2} \geq 0$ and all zeros for the other $(n_1 - n_2)$ rows.

First, the singular values of $\mathbf{\Phi}_{\mathrm{p}}^{''\mathrm{d}}$ can be used to indicate the presence of damage. The reason is that the mode shape curvature of pristine structures could be approximated by the first several principal components while the damage increases the active principal components or rank of the mode shape curvature matrix. Figure 1 depicts the singular value plot of the 10th mode shape curvature of a plate in the cases of no damage and two damage zones with different damage severities, which demonstrates that there will be more large singular values when damage is present. However, it seems that the singular values are not very sensitive to the damage zones with different levels of severity at the same location.

Second, it is possible to localise the damage using matrix $\mathbf{E}$.[16] The approximation of $\mathbf{\Phi}_{\mathrm{p}}^{''}$ is obtained by using the first several singular values $k(k < n_2)$ and singular vectors.

$$\widehat{\mathbf{\Phi}}_{\mathrm{p}}^{''} = \mathbf{L} = \mathbf{U}\widetilde{\mathbf{\Sigma}}\mathbf{V}^{\mathrm{T}};\ \widetilde{\mathbf{\Sigma}} = \mathrm{diag}[\lambda_1, \lambda_2, \cdots, \lambda_k, 0,\ \ 0, \cdots, 0], \tag{10}$$

where the diagonal entries of $\widetilde{\mathbf{\Sigma}}$ are comprised of the first k singular values and zeros for the others. Therefore, matrix $\mathbf{E}$ is determined as

$$\mathbf{E} = \mathbf{\Phi}_{\mathrm{p}}^{''\mathrm{d}} - \widehat{\mathbf{\Phi}}_{\mathrm{p}}^{''}. \tag{11}$$

In the process of evaluating $\widehat{\mathbf{\Phi}}^{''}$, any grossly corrupted (outlier) entries in $\mathbf{\Phi}_{\mathrm{p}}^{''\mathrm{d}}$ could cause the estimation of $\widehat{\mathbf{\Phi}}_{\mathrm{p}}^{''}$ arbitrarily far from the true $\mathbf{\Phi}_{\mathrm{p}}^{''}$.[40] However, it is common to have grossly corrupted entries in $\mathbf{\Phi}_{\mathrm{p}}^{''\mathrm{d}}$, which are caused by damage or measurement noise. In order to improve the damage localisation accuracy of PCA, a robust PCA is studied next.

3.2 | Robust PCA

Robust PCA aims to estimate the low-rank $\mathbf{L}$ based on the grossly corrupted $\mathbf{\Phi}_{\mathrm{p}}^{''\mathrm{d}}$. In robust PCA, the decomposition of $\mathbf{\Phi}_{\mathrm{p}}^{''\mathrm{d}}$ into a low-rank matrix $\mathbf{L}$ plus a sparse component $\mathbf{S}$ can be achieved by several approaches such as principal

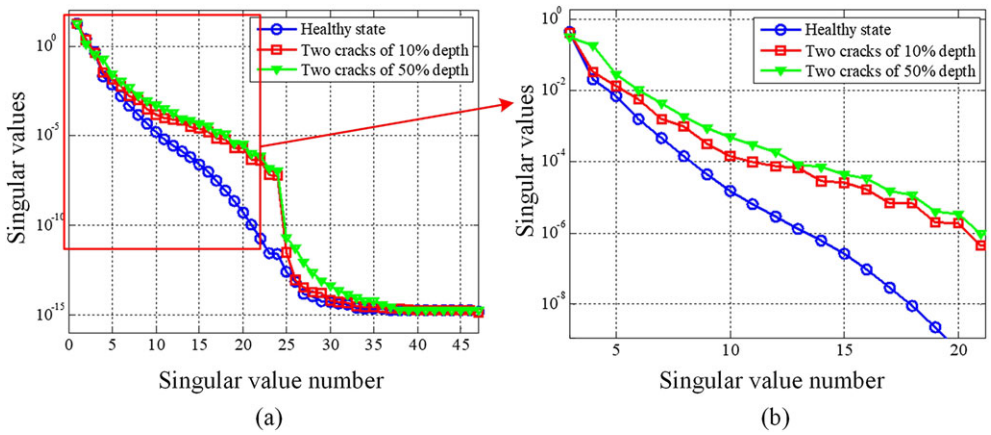

FIGURE 1 Singular value plot of the 10th mode shape curvature of a plate without damage and with two damage areas of different depths based on the numerical study

component pursuit (PCP), outlier pursuit and iteratively reweighted least-squares.[42] According to PCP, the problem is expressed as

$$\text{minimise } \|\mathbf{L}\|_* + \xi\|\mathbf{S}\|_1 \quad \text{subject to } \mathbf{L}+\mathbf{S} = \mathbf{\Phi}_{\mathrm{p}}^{''\mathrm{d}}, \tag{12}$$

where ξ is a balance parameter, $\|\mathbf{L}\|_* = \sum_i \lambda_i(\mathbf{L})$ represents the nuclear norm of matrix $\mathbf{L}$ (which is the ℓ_1 norm of singular values), and $\|\mathbf{S}\|_1 = \sum_{ij}|s_{ij}|$ denotes the ℓ_1 norm of matrix $\mathbf{S}$.

For damage identification, $\mathbf{L}$ corresponds to the mode shape curvature $\mathbf{\Phi}_{\mathrm{p}}^{''}$ of the healthy state whereas $\mathbf{S}$ is associated with damage-induced components. However, $\mathbf{\Phi}_{\mathrm{p}}^{''\mathrm{d}}$ is always contaminated by measurement noise and the measurement noise can be stochastic or deterministic. Hence, the entry-wise noise of $\mathbf{\Phi}_{\mathrm{p}}^{''\mathrm{d}}$ should be considered to guarantee a robust and accurate solution of $\mathbf{S}$. The new PCP by considering the noise effects is modelled as

$$\text{minimise } \|\mathbf{L}\|_* + \xi\|\mathbf{S}\|_1 \quad \text{subject to } \left\|\mathbf{\Phi}_{\mathrm{p}}^{''\mathrm{d}} - \mathbf{L} - \mathbf{S}\right\| \le \epsilon, \tag{13}$$

where the constraint in Equation (12) is relaxed as $\left\|\mathbf{\Phi}_{\mathrm{p}}^{''\mathrm{d}} - \mathbf{L} - \mathbf{S}\right\| \le \epsilon$ ($\epsilon > 0$), and ξ is set as $1/\sqrt{\max(n_1, n_2)}$.[43] This PCP problem is addressed efficiently by convex optimisation algorithms and encouraging performance has been demonstrated on face images and background modelling.[44]

In Equation (13), the minimisation of $\|\mathbf{L}\|_*$ and $\|\mathbf{S}\|_1$ implies that $\mathbf{L}$ is approximated by a low-rank subspace whereas the damage-caused mode shape curvature changes are contained in sparse matrix $\mathbf{S}$. If rank($\mathbf{L}$) is too high, $\mathbf{L}$ will incorporate the damage features in its representation. If rank($\mathbf{L}$) is too low, some mode shape curvature features will appear in $\mathbf{S}$, which will corrupt the damage identification procedure and even produce misleading identification results. Therefore, the balance parameter ξ should be chosen appropriately to well separate the low-rank and sparse matrices.

The challenging problem of applying robust PCA for damage identification is that robust PCA is normally used in the pixel domain based on images or videos. But the mode shape curvature $\mathbf{\Phi}_{\mathrm{p}}^{''\mathrm{d}}$ of a plate in this study is acquired from discrete measurement points by SLV. The spatial resolution of measurement points is much lower than an image, which increases the difficulties of applying robust PCA. Thus, the feasibility and the effectiveness of applying robust PCA to damage identification based on discrete mode shapes remain to be seen.

4 | ROBUST MULTIDAMAGE INDEX

With the estimated sparse matrix $\mathbf{S}$, a robust multidamage index is proposed based on a statistical criterion. First, the value s_{ij} associated with each measurement point is regarded as a random value realisation. Then, the normalised mode shape curvature difference is defined as

$$\widetilde{s}_{ij} = \left(s_{ij} - \bar{s}\right)/\sigma_{\mathrm{s}}, \tag{14}$$

where $\bar{s}$ and σ_{s} denote the mean value and standard deviation of all entries in $\mathbf{S}$.

Normally, the outlier values of $\widetilde{\mathbf{S}}$ (large positive or negative values) are used to indicate the damage locations. To get rid of other smaller values of $\widetilde{\mathbf{S}}$ due to measurement noise, a robust damage localisation is conducted by testing a statistical hypothesis. The null hypothesis (H_0) is that the damage does not occur at the lth measurement point, and its alternative hypothesis H_1 states that the damage occurs at the lth measurement point. Thus, the damage localisation is to determine the confidence probability to accept H_1 or reject H_0.[45]

Simply, a threshold value $\widetilde{s}_{\alpha/2}$ (α represents the percentile) can be selected, and the damage locations are determined as

$$\left|\widetilde{s}_{ij}\right| \ge \widetilde{s}_{\alpha/2}, \tag{15}$$

In Equation (15), the α value is determined according to the three-sigma limits of a normal distribution. For a pristine structure, the elements in the sparse matrix $\mathbf{S}$ mostly locate in the range of $\left[\mu - 3\sigma_{\widetilde{s}}, \mu + 3\sigma_{\widetilde{s}}\right]$, where $\mu(\mu = 0)$ and $\sigma_{\widetilde{s}}\left(\sigma_{\widetilde{s}} = 1\right)$ are the mean value and standard deviation of all the entries in the normalised $\widetilde{\mathbf{S}}$. The outlier values located outside this range tend to be scattered over the plate surface. However, the presence of damage leads to more outlier values that locate outside $\left[\mu - 3\sigma_{\widetilde{s}}, \mu + 3\sigma_{\widetilde{s}}\right]$, which tend to be spatially close to each other around the damage.

Therefore, the outlier values that locate outside the three standard deviations from the mean ($\widetilde{s}_{\alpha/2} = \mu + 3\sigma_{\widetilde{s}}$ and $\alpha = 0.0027$) are taken for damage localisation.

For $|\widetilde{s}_{ij}| < \widetilde{s}_{\alpha/2}$, there is no damage, and the associated $\widetilde{s}_{ij}$ is set as zero. Thus, for a certain mode shape, the updated damage-induced mode shape curvature changes are

$$\widetilde{s}_{ij} = \begin{cases} |\widetilde{s}_{ij}|, \ |\widetilde{s}_{ij}| \geq \widetilde{s}_{\alpha/2} \\ 0, \ |\widetilde{s}_{ij}| < \widetilde{s}_{\alpha/2} \end{cases}. \tag{16}$$

For the curvatures of N_r modes, a robust multidamage index is defined as

$$DI_{ij} = \frac{1}{N_r} \sum_{r=1}^{N_r} \widetilde{s}_{ij}^{\,r}. \tag{17}$$

To demonstrate the concept of robust multidamage localisation, several mode shapes are used, as they are the representative structural CDSs. In practice, operational deflection shapes at several nonresonant frequencies can also be employed for robust damage identification.

5 | NUMERICAL SIMULATIONS

A cantilever aluminium plate of dimension 0.35 × 0.23 × 0.003 m^3 with Young's modulus E = 69 GPa, Poisson's ratio ν = 0.35, and mass density ρ = 2,700 kg/m^3 is studied. The plate is modelled using four-node quadrilateral elements in MATLAB according to Mindlin plate theory. The cantilever plate is discretised into 70 × 46 elements with each element of 0.005 × 0.005 × 0.003 m^3, and the clamped edge is located on the left. Here, two damage cases of a plate with two damage zones are studied, which are shown in Figure 2. For Numerical case 1, the two damage positions are centred at (0.10 m, 0.115 m) and (0.21 m, 0.115 m) with an equal area of 0.02 × 0.02 m^2. For Numerical case 2, the two damage positions are centred at (0.155 m, 0.0075 m) and (0.155 m, 0.155 m) with an equal area of 0.02 × 0.02 m^2. In both cases, the damage areas have a reduced thickness of 10% with respect to the pristine plate. To better mimic practical experiments, Gaussian white noise is generated to contaminate the mode shape data in the form of

$$\widetilde{\Phi}_r(x,y) = \Phi_r(x,y) + n_n n_{level} \sigma(\Phi_r(x,y)), \tag{18}$$

where $\Phi_r(x,y)$ denotes the rth mode shape with x and y indicating the location, $\widetilde{\Phi}_r(x,y)$ represents the noisy mode shape value, and n_n is the normally distributed random white noise with a zero-mean value and a variance being 1. In addition, n_{level} is the noise level range of [0, 1], and $\sigma(\Phi_r(x,y))$ indicates the standard variance of the rth mode shape.

In the following study, the 10th mode shape that is sensitive to the two damage locations of Numerical case 1 is first used to demonstrate the noise robustness of the estimated curvatures by LoG filter and the better damage localisation performance of robust PCA method. Then, the 10th mode shape is verified to be ineffective in the damage localisation of

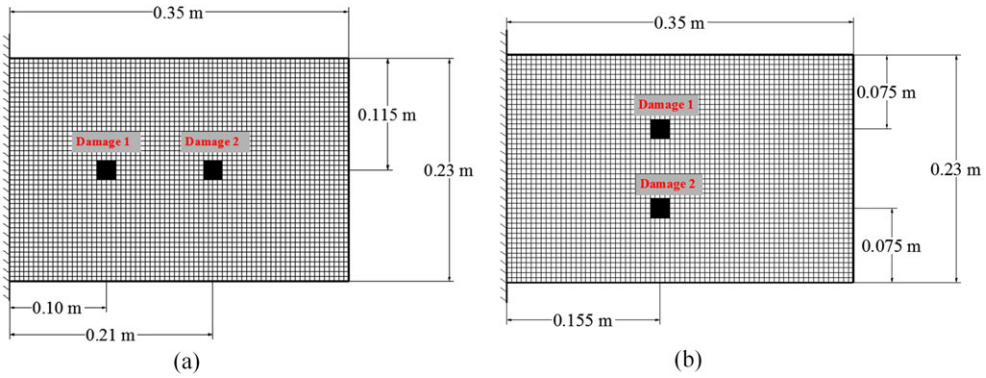

FIGURE 2 FE model of a plate with two damaged zones: (a) Case 1 and (b) Case 2

Numerical case 2, and hence, the integration of damage information of more than one mode (six modes in these particular cases) is proved to be necessary for a robust multidamage identification.

Gaussian white noise of n_{level} = 0.1% (signal to noise ratio (SNR) = 60.10 dB) is added to pollute the 10th mode shape of Numerical case 1. Then, the mean *x-y* curvature of the 10th mode shape is estimated by the second-order central difference approach and LoG filter with σ=1, 1.5, 2, respectively, which are displayed in Figure 3.

Figure 3 depicts that the second-order central difference approach is significantly affected by the measurement noise whereas LoG filter is good at processing the noisy mode shape. Second, by comparing Figure 3b with Figure 3d, it is apparent that the damage-induced shape singularities decrease when increasing the scale parameter σ. Thus, an appropriate scale parameter should be used to supress the measurement noise while keeping the damage-induced shape singularities. Here, σ = 1.5 is used to reduce the noise effects while keeping the effective damage information. The damage localisation results of Numerical case 1 by using traditional PCA and robust PCA are given in Figure 4.

In Figure 4, the pink rectangles indicate the actual damage areas. It is clear that the traditional PCA is unable to localise the two damage zones whereas the robust PCA is accurate in detecting the two damage locations. Then, the mean *x-y* curvature of the 10th mode shape is used to identify the two damage areas of Numerical case 2 via the robust PCA, and the damage localisation results are presented in Figure 5.

Figure 5 indicates that the two damage areas cannot be localised by using the 10th mode shape curvature, which shows that a single mode shape is not robust for multidamage localisation. Therefore, a robust multidamage localisation method should incorporate the damage information of several mode shapes together. To achieve this, mean *x-y* curvatures of the 10th to 15th mode shapes are used to evaluate the proposed robust damage index for the two numerical cases, and the damage localisation results are illustrated in Figure 6. In addition, the mode shapes from 10th to 15th are contaminated by 0.1% Gaussian white noise before evaluating their mean *x-y* curvatures. In Figure 6, the two damage zones with 10% thickness reduction of both numerical cases can be correctly localised, which demonstrates the effectiveness of the proposed multidamage index.

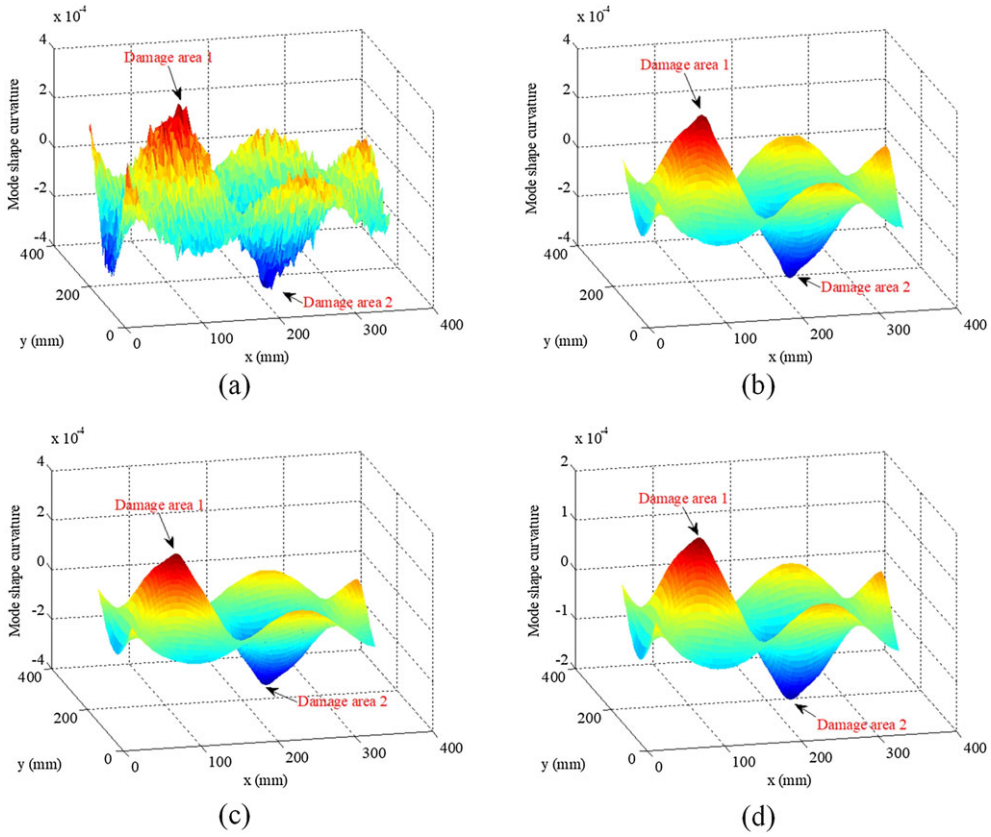

FIGURE 3 Mean *x-y* curvature of Numerical case 1: (a) second-order central difference, (b) Laplacian of Gaussian (LoG) filter with σ = 1, (c) LoG filter with σ = 1.5, and (d) LoG filter with σ = 2

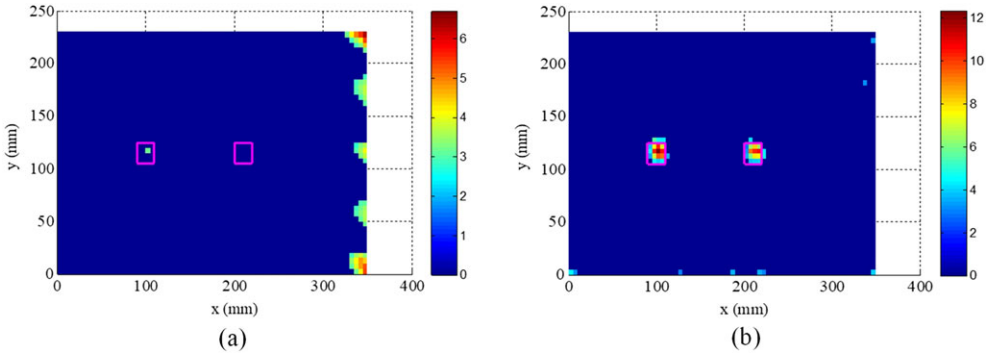

FIGURE 4 Damage localisation results of Numerical case 1: (a) traditional principal component analysis (PCA) and (b) robust PCA

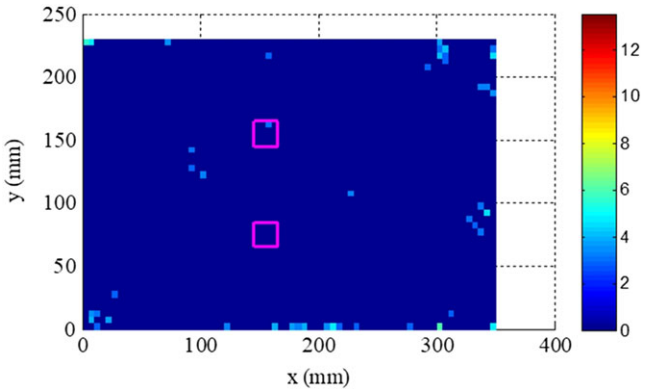

FIGURE 5 Damage localisation results of Numerical case 2 based on robust principal component analysis

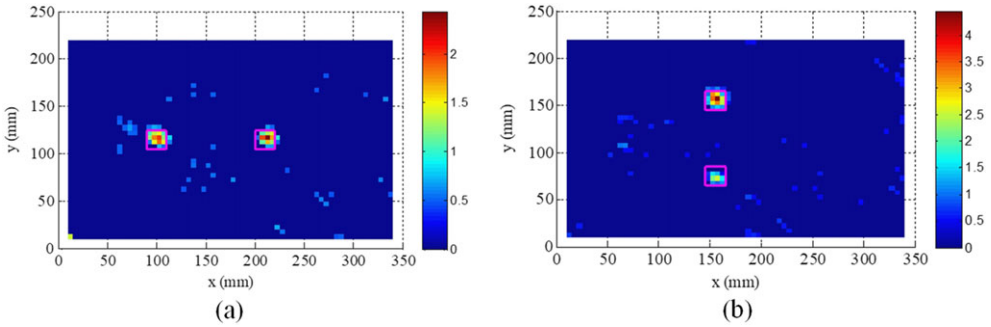

FIGURE 6 Robust multidamage localisation results based on robust principal component analysis: (a) Numerical case 1 and (b) Numerical case 2

6 | EXPERIMENTAL SET-UP AND ANALYSIS

In order to verify the robust mode shape curvature estimation approach and the proposed robust multidamage index in practical applications, cantilever aluminium plates with the same physical and geometrical properties as those used in the numerical study are tested. The experimental set-up is illustrated in Figure 7. Ten percent of the thickness on the opposite side of the two damage areas marked as two small squares are cut off, and their position coordinates are given in Figure 2. In addition, the plate is clamped on the left and excited by a shaker (LDS V406) on the right.

The vibration responses are measured by a PSV-500 SLV, and the measured zone is slightly smaller than the original plate dimensions to avoid the effects of boundaries. For example, the measurement zone is 0.326m × 0.219 m spanning from 0.0084 to 0.3334 m in the x direction and 0.0028 to 0.2218 m in the y direction for Experimental case 1 as given in

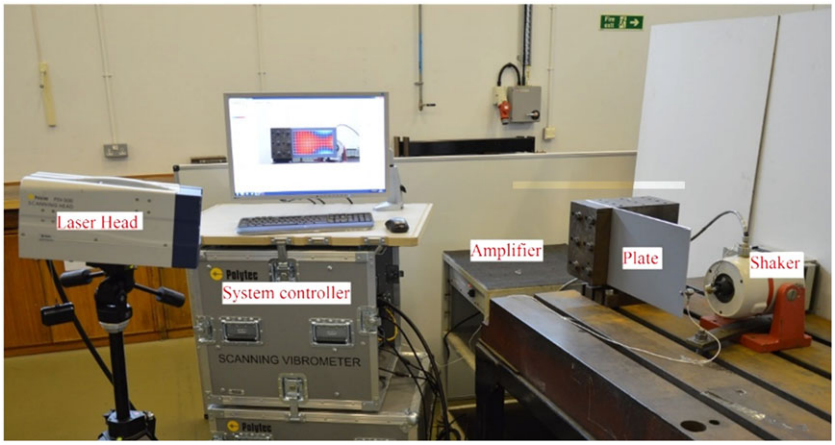

FIGURE 7 Experimental set-up of a cantilever plate

Figure 8a. Moreover, there are 141 × 95 measurement points with grid cell size of 0.00233m × 0.00233 m. In addition, the measurement zone of Experimental case 2 is shown in Figure 9a.

To determine the resonant frequencies of the plate, a pseudorandom signal of 0–2,000 Hz is used to excite the plate, which is generated by the PSV-500 system. After the resonant frequencies are obtained from the frequency response function, the plate will be excited at a certain resonant frequency to acquire its associated mode shape data.

Take the Experimental case 1 for example, the 10th resonant frequency at 798 Hz is used to excite the plate, and the velocities of the measurement grid are acquired. The "FastScan" mode of PSV-500 is selected to measure the mode shape due to its fast acquisition efficiency. In this mode, the specific excitation frequency is set as 798 Hz, and the bandwidth of acquisition signal is set as 300 Hz. A wider bandwidth can speed up the measurement, whereas a narrow bandwidth will provide a better signal-to-noise ratio. For this experiment, 30 averages were used, and the total measurement time is around 30 min. In addition, 40 averages were also investigated, but it did not further enhance the measurement accuracy. Figure 10 presents the measured 10th mode shape, which is normalised with its value range of [−1, 1]. The mean *x-y* curvature of the 10th mode shape is shown in Figure 11.

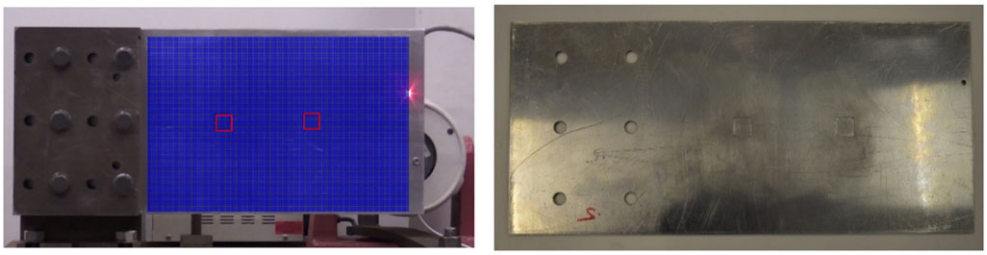

FIGURE 8 Experimental case 1 of a cantilever plate with two damage zones: (a) front surface view and (b) back surface view

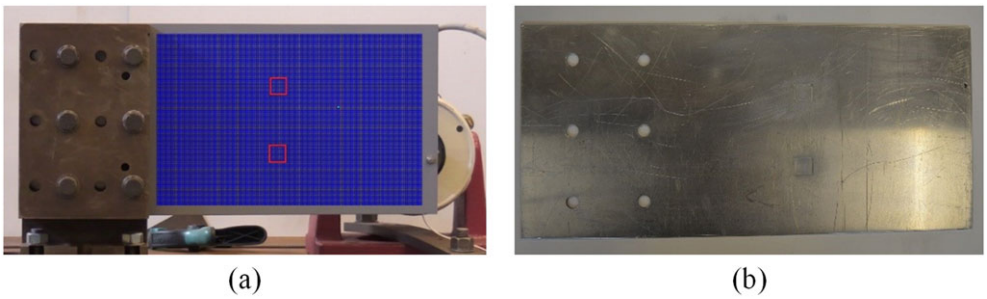

FIGURE 9 Experimental case 2 of a cantilever plate with two damage zones: (a) front surface view and (b) back surface view

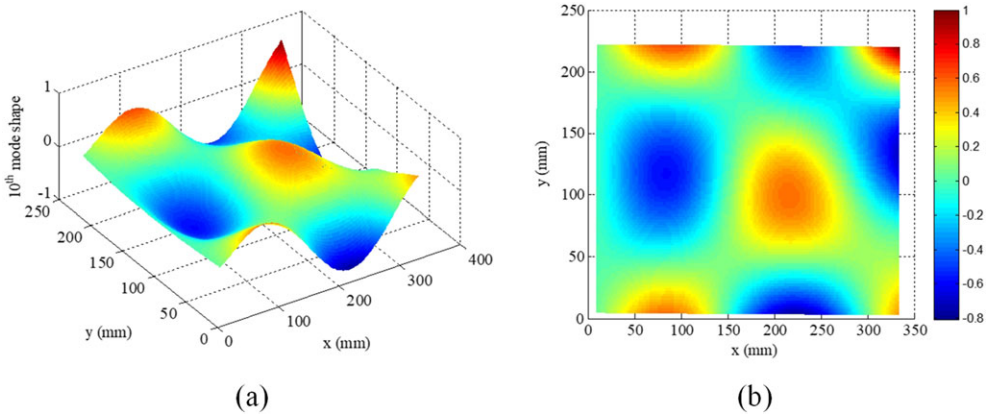

FIGURE 10 The normalised 10th mode shape of Experimental case 1

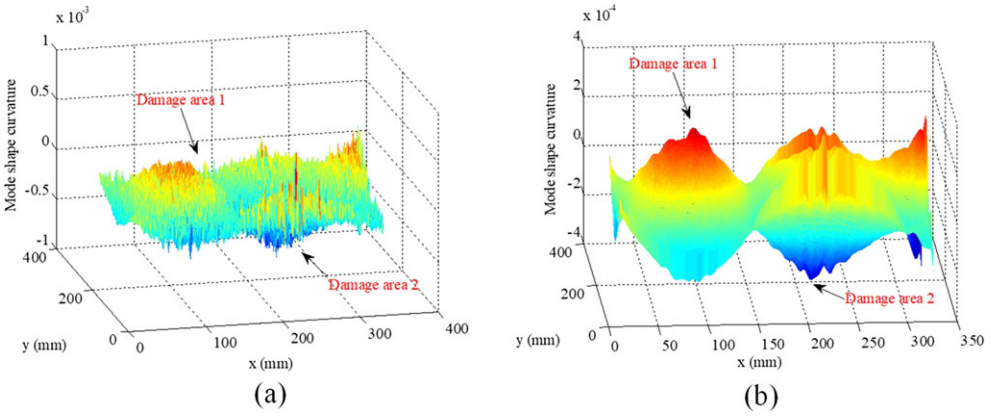

FIGURE 11 Mean *x*-*y* curvature of Experimental case 1: (a) second-order central difference approach and (b) Laplacian of Gaussian filter with $\sigma = 1.5$

Clearly, without denoise processing, it is hard to obtain useful information for damage identification as shown in Figure 11a. By applying the LoG filter, the estimated curvatures are much smoother. Nevertheless, they are still affected by the measurement noise. Apart from the scale parameter of the LoG filter, there is another important parameter that can be adjusted to reduce the measurement noise, which is the grid distance between two successive measurement points. During the data acquisition phase, the grid distance is determined by the measurement density. However, the grid distance of measurement points can be adjusted after data acquisition by interpolation approaches. Therefore, a relatively high measurement density is commonly used for data acquisition in experiments.

Here, in order to further enhance the noise robustness of experimental data, triangulation-based linear interpolation is adopted to increase the grid distance of measurement points. Originally, there are 141 × 95 measurement points covering the measurement zone. Now, based on these data, a 80 × 54 grid is assigned, and the mode shape value of each point is evaluated by the linear interpolation. For more information, please refer to the "griddata" function in MATLAB. After interpolation of the original data, the curvature is recalculated and presented in Figure 12.

It demonstrates that by appropriately increasing the grid distance, the estimated curvatures tend to be less susceptible to the measurement noise and more sensitive to damage. Now, with the estimated noise robust mode shape curvature, the proposed robust multidamage identification approach based on robust PCA is implemented for accurate damage localisation, and the results are given in Figure 13.

It can be seen that the 10th mode shape is unable to identify the two damage positions of Experimental case 2. To overcome this shortcoming, more mode shapes should be used to provide sensitive and effective damage localisation spanning all the measured zone. To demonstrate this idea, the damage information of the 10th and 13th mode shapes is combined to form a robust multidamage index, and the damage localisation results for two exerpimental cases based on robust PCA are presented in Figure 14.

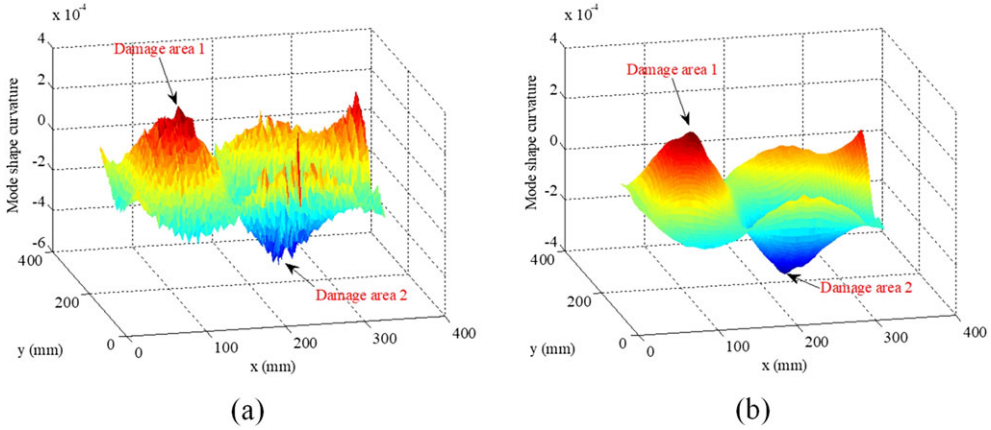

FIGURE 12 Improved mean *x-y* curvature of Experimental case 1: (a) second-order central difference approach and (b) Laplacian of Gaussian filter with $\sigma = 1.5$

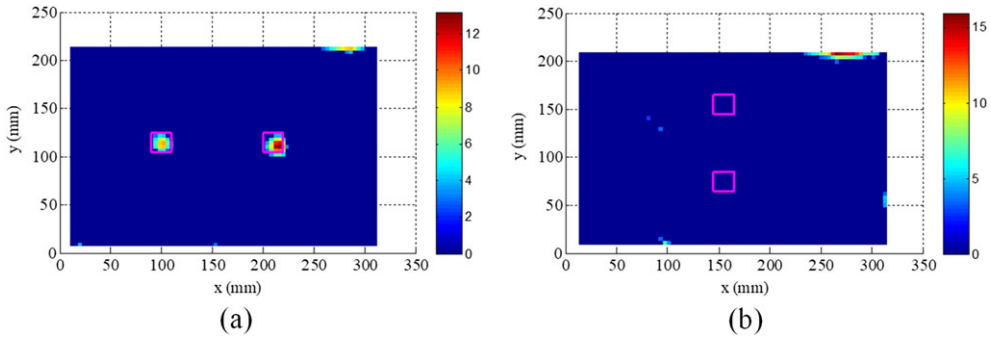

FIGURE 13 Damage localisation results based on the 10th mode shape curvature: (a) Experimental case 1 and (b) Experimental case 2

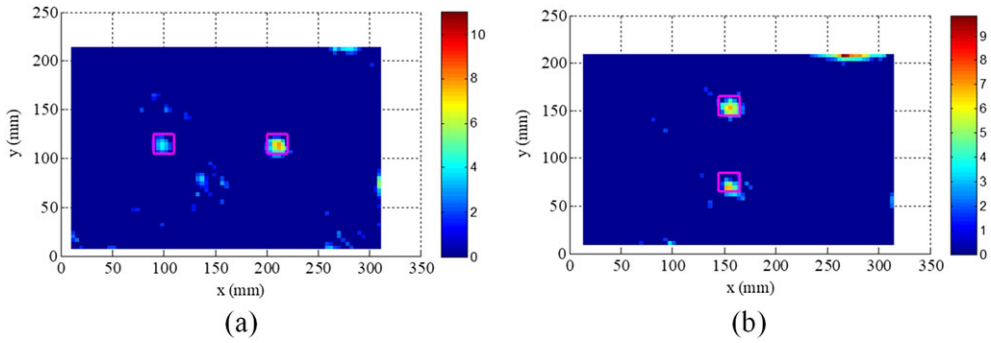

FIGURE 14 Robust multidamage localisation results: (a) Experimental case 1 and (b) Experimental case 2

It is clear that the multidamage index based on the 10th and 13th mode shapes is robust and able to localise the two damage zones of both experimental cases. However, in practical applications, the damage information is not known in advance, and more mode shapes should be incorporated in the multidamage index, which is a central idea of the presented method.

7 | CONCLUSIONS

In this paper, a baseline-free multidamage identification method is proposed by evaluating the local damage-induced structural property changes in plate-type structures. It is a data-driven approach, and the low-rank structure of mode shape curvatures is used for damage detection and localisation without requiring the theoretical model and baseline

information of the structures. Moreover, investigations are carried out in three aspects to boost its efficiency and effectiveness, which are robust curvature estimation, robust damage feature extraction, and robust multidamage localisation index.

Two numerical case studies of a plate with two damage areas coded in MATLAB are used to assess the performance of the proposed baseline-free multidamage identification method under idealised conditions. Moreover, Gaussian white noise is added to contaminate the mode shape data in numerical studies to simulate the practical measurement noise. Experimental studies of plates with two damage areas identical to the plate in the numerical simulations are also tested to experimentally validate the proposed baseline-free multidamage identification method. Finally, the major conclusions are summarised as follows:

a. The LoG filter is demonstrated to be much more noise robust in curvature estimation when compared with the traditional second-order central difference method.
b. The robust PCA is shown to be much more effective in extracting damage-induced local shape singularities than the traditional PCA.
c. The proposed multidamage index is proved to be sensitive to damage at various possible locations when the damage information of several modes is used.
d. Apart from the scale parameter of LoG filter, the distance between adjacent measurement points can also be tuned to reduce the effects of measurement noise.

ACKNOWLEDGEMENTS

This work was carried out in the School of Engineering, University of Liverpool while the first author was studying as a PhD student sponsored by a UoL-CSC Scholarship.

ORCID


Huajiang Ouyang https://orcid.org/0000-0003-0312-0326

REFERENCES

1. Montalvao D, Maia NMM, Ribeiro AMR. A review of vibration-based structural health monitoring with special emphasis on composite materials. *Shock Vib Dig*. 2006;38(4):295-326.
2. Cao M, Sha G, Gao Y, Ostachowicz W. Structural damage identification using damping: a compendium of uses and features. *Smart Mater Struct*. 2017;26(4):043001.
3. Lin X, Yuan F. Detection of multiple damages by prestack reverse-time migration. *AIAA J*. 2001;39(11):2206-2215.
4. Inman DJ, Farrar CR, Junior VL, Junior VS. *Damage Prognosis: For Aerospace, Civil and Mechanical Systems*. John Wiley & Sons; 2005.
5. Xu H, Cheng L, Su Z, Guyader JL. Identification of structural damage based on locally perturbed dynamic equilibrium with an application to beam component. *J Sound Vib*. 2011;330(24):5963-5981.
6. Farrar CR, Worden K. *Structural Health Monitoring: A Machine Learning Perspective*. John Wiley & Sons; 2012.
7. Doebling SW, Farrar CR, Prime MB. A summary review of vibration-based damage identification methods. *Shock Vib Dig*. 1998;30(2):91-105.
8. Yao Y, Tung STE, Glisic B. Crack detection and characterization techniques—an overview. *Struct Control Health Monit*. 2014;21(12):1387-1413.
9. Xu Y, Zhu W. Non-model-based damage identification of plates using measured mode shapes. *Struct Health Monit*. 2016;16:3-23.
10. Xu W, Radzieński M, Ostachowicz W, Cao M. Damage detection in plates using two-dimensional directional Gaussian wavelets and laser scanned operating deflection shapes. *Struct Health Monit*. 2013;12(5-6):457-468.
11. Li Y, Cheng L, Yam L, Wong W. Identification of damage locations for plate-like structures using damage sensitive indices: strain modal approach. *Comput Struct*. 2002;80(25):1881-1894.
12. Garcia D, Palazzetti R, Trendafilova I, Fiorini C, Zucchelli A. Vibration-based delamination diagnosis and modelling for composite laminate plates. *Compos Struct*. 2015;130:155-162.

13. Wang L, Yuan F. Damage identification in a composite plate using prestack reverse-time migration technique. *Struct Health Monit*. 2005;4(3):195-211.
14. Lin X, Yuan F. Damage detection of a plate using migration technique. *J Intell Mater Syst Struct*. 2001;12(7):469-482.
15. Rucevskis S, Janeliukstis R, Akishin P, Chate A. Mode shape-based damage detection in plate structure without baseline data. *Struct Control Health Monit*. 2016;23(9):1180-1193.
16. Jiang Y, Xiang J, Li B, Chen X, Lin L. A hybrid multiple damages detection method for plate structures. *Sci China Technol Sci*. 2017;60(5):726-736.
17. Douka E, Loutridis S, Trochidis A. Crack identification in plates using wavelet analysis. *J Sound Vib*. 2004;270(1-2):279-295.
18. Wu D, Law SS. Damage localization in plate structures from uniform load surface curvature. *J Sound Vib*. 2004;276(1-2):227-244.
19. Hadjileontiadis LJ, Douka E. Crack detection in plates using fractal dimension. *Eng Struct*. 2007;29(7):1612-1625.
20. Qiao P, Lu K, Lestari W, Wang J. Curvature mode shape-based damage detection in composite laminated plates. *Compos Struct*. 2007;80(3):409-428.
21. Grediac M. The use of full-field measurement methods in composite material characterization: interest and limitations. *Compos a: Appl Sci Manuf*. 2004;35(7-8):751-761.
22. Wang W, Mottershead JE, Mares C. Vibration mode shape recognition using image processing. *J Sound Vib*. 2009;326(3-5):909-938.
23. Speranzini E, Agnetti S. The technique of digital image correlation to identify defects in glass structures. *Struct Control Health Monit*. 2014;21(6):1015-1029.
24. Cao S, Ouyang H. Output-only damage identification using enhanced structural characteristic deflection shapes and adaptive gapped smoothing method. *J Vib Acoust*. 140(2018):011005.
25. Zhang C, Cheng L, Xu H, Qiu J. Structural damage detection based on virtual element boundary measurement. *J Sound Vib*. 2016;372:133-146.
26. Lopes H, Ferreira F, Araújo dos Santos JV, Moreno-García P. Localization of damage with speckle shearography and higher order spatial derivatives. *Mech Syst Signal Process*. 2014;49(1-2):24-38.
27. Xu W, Cao M, Ostachowicz W, Radzieński M, Xia N. Two-dimensional curvature mode shape method based on wavelets and Teager energy for damage detection in plates. *J Sound Vib*. 2015;347:266-278.
28. Chang CC, Chen LW. Damage detection of a rectangular plate by spatial wavelet based approach. *Appl Acoust*. 2004;65(8):819-832.
29. Lam HF, Yin T. Application of two-dimensional spatial wavelet transform in the detection of an obstructed crack on a thin plate. *Struct Control Health Monit*. 2012;19(2):260-277.
30. Pandey AK, Biswas M, Samman MM. Damage detection from changes in curvature mode shapes. *J Sound Vib*. 1991;145(2):321-332.
31. Hu C, Afzal MT. A statistical algorithm for comparing mode shapes of vibration testing before and after damage in timbers. *J Wood Sci*. 2006;52(4):348-352.
32. Wahab MMA, De Roeck G. Damage detection in bridges using modal curvatures: application to a real damage scenario. *J Sound Vib*. 1999;226(2):217-235.
33. Surace C, Saxena R, Gherlone M, Darwich H. Damage localisation in plate like-structures using the two-dimensional polynomial annihilation edge detection method. *J Sound Vib*. 2014;333(21):5412-5426.
34. Cao M, Xu W, Ren WX, Ostachowicz W, Sha GG, Pan LX. A concept of complex-wavelet modal curvature for detecting multiple cracks in beams under noisy conditions. *Mech Syst Signal Process*. 2016;76:555-575.
35. Yoon MK, Heider D, Gillespie JW, Ratcliffe CP, Crane RM. Local damage detection using the two-dimensional gapped smoothing method. *J Sound Vib*. 2005;279(1-2):119-139.
36. Yang Y, Sun P, Nagarajaiah S, Bachilo SM, Weisman RB. Full-field, high-spatial-resolution detection of local structural damage from low-resolution random strain field measurements. *J Sound Vib*. 2017;399:75-85.
37. Tondreau G, Deraemaeker A. Multi-scale modal filters for early damage localization. In: International Conference on Noise and Vibration Engineering; 2012, pp. 881–892; Leuven, Belgium.
38. Moreno-García P, dos Santos JA, Lopes H. A new technique to optimize the use of mode shape derivatives to localize damage in laminated composite plates. *Compos Struct*. 2014;108:548-554.
39. Lindeberg T. *Scale-space Theory in Computer Vision*. Springer Science & Business Media; 2013.
40. Candès EJ, Li X, Ma Y, Wright J. Robust principal component analysis? *J ACM*. 2011;58:11.
41. Nagarajaiah S, Yang Y. Modeling and harnessing sparse and low-rank data structure: a new paradigm for structural dynamics, identification, damage detection, and health monitoring. *Struct Control Health Monit*. 2017;24(1).
42. Bouwmans T, Zahzah EH. Robust PCA via principal component pursuit: a review for a comparative evaluation in video surveillance. *Comput Vis Image Underst*. 2014;122:22-34.

43. Zhou Z, Li X, Wright J, Candes E, Ma Y. Stable principal component pursuit.In: Proceedings IEEE International Symposium on Information Theory Austin; 2010, pp. 1518–1522; Texas, USA.

44. De la Torre F, Black MJ. Robust principal component analysis for computer vision. In: Proceedings Eighth IEEE International Conference on Computer Vision; 2001, pp. 362–369; Vancouver, Canada.

45. Kim JT, Stubbs N. Damage localization in structures without baseline modal parameters. *AIAA J*. 1996;34:1644-1649.

How to cite this article: Cao S, Ouyang H, Cheng L. Baseline-free multidamage identification in plate-like structures by using multiscale approach and low-rank modelling. *Struct Control Health Monit*. 2018;e2293. https://doi.org/10.1002/stc.2293